Journal of Power Sources 269 (2014) 834–840

Contents lists available at ScienceDirect

Journal of Power Sources

journal homepage: www.elsevier.com/locate/jpowsour

Optimized electrode arrangement and activation of bioelectrodes activity by carbon nanoparticles for efficient ethanol microfluidic biofuel cells

D. Selloum [a, b], S. Tingry [a, *], V. Techer [a], L. Renaud [c], C. Innocent [a], A. Zouaoui [b]

[a] Institut Européen des Membranes, UMR 5635, ENSCM-UMII-CNRS, place Eugène Bataillon, 34095 Montpellier, France
[b] Laboratoire de Croissance et Caractérisation de Nouveaux Semiconducteurs (LCCNS), Faculté de Technologie, Université Sétif 1, Sétif 19000, Algeria
[c] Université de Lyon, Institut des Nanotechnologies de Lyon INL-UMR5270, CNRS, Université Lyon 1, Villeurbanne F-69622, France

HIGHLIGHTS

- Development of the first ethanol microfluidic biofuel cell based on bioelectrodes.
- Device optimized as function of electrode patterns in the microfluidic channel.
- Shorter and wider electrodes delivered higher current and power densities.
- Carbon nanoparticles with higher porosity enhanced bioelectrocatalytic processes.
- The miniature biofuel cell generated maximum power density of 90 μW cm^{-2} at 0.6 V.

ARTICLE INFO

Article history:
Received 1 April 2014
Received in revised form
19 June 2014
Accepted 9 July 2014
Available online 17 July 2014

Keywords:
Microfluidics
Carbon nanoparticles
Bioelectrodes
Enzyme kinetics
Enzymatic biofuel cell

ABSTRACT

This work presents the construction of an ethanol microfluidic biofuel cell based on a biocathode and a bioanode, and operating in a Y-shaped microfluidic channel. At the anode, ethanol was oxidized by alcohol dehydrogenase, whereas at the cathode, the oxygen was reduced by laccase. Fuel and oxidant streams moved in parallel laminar flow without turbulent mixing into a microchannel fabricated using soft lithography methods. The enzymes were immobilized in the presence of reactive species at gold electrode surfaces. Bioelectrocatalytic processes were enhanced by combination of enzymes and carbon nanoparticles, attributed to appropriate electron transport and high amount enzyme loading. The benefit of the nanoparticles with higher surface porosity was explained by the high porous structure that offered a closer proximity to the reactive species and improved diffusion of the substrates within the enzyme films. The microfluidic BFC was optimized as function of electrode patterns, showing that higher current and power densities were achieved for shorter and wider electrodes that allow for thinner boundary layer depletion at the electrodes surface resulting in efficient catalytic consumption of fuel and oxidant. This miniaturized device generated maximum power density of 90 μW cm^{-2} at 0.6 V for a flow rate 16 μL min^{-1}.

1. Introduction

Recent increasing demands on small-scale sources for portable electronics have significantly boosted the interest in miniaturized fuel cells. Microfluidic techniques have been used for miniaturization of these devices based on microfluidic channels of submilliter in height [1]. Combination of microfluidic technologies and biological materials (enzymes) has given rise to the development of microfluidic biofuel cells [2–5]. These devices used enzymes as catalysts to convert chemical energy into electricity [6]. The components of these devices are analogous of the conventional microfluidic fuel cells based on anodic and cathodic compartments [1,7,8]. Fuel and oxidant streams move in parallel laminar flow without turbulent mixing into a microchannel fabricated using soft lithography methods [9]. These devices operate without the need of a separation membrane allowing for different pHs at the anolyte

* Corresponding author. Tel.: +33 (0)4 67 14 91 57; fax: +33 (0)4 67 14 91 19.
E-mail addresses: sophie.tingry@univ-montp2.fr, sophie.tingry@iemm.univ-montp2.fr (S. Tingry).

http://dx.doi.org/10.1016/j.jpowsour.2014.07.052
0378-7753/

and the catholyte for optimal kinetics reaction. The mixing of the flows can only occur through diffusion, restricted to a thin interfacial zone in the center of the channel [1,10].

An important step to construct biofuel cells is the immobilization of enzymes on conductive support to ensure their electrical contact with electrodes and limit their denaturation. Electrodes modified by enzymes are the subject to develop prospective bioelectrodes to deliver high catalytic current density [11]. However, current densities are limited by low coverage of enzymes on the electrodes, low stability and sluggish electron transfer. The use of conductive nanomaterials with remarkable surface properties, like carbon nanotubes or nanoparticles, for bioelectrode modification provides an alternative and frequently used option to increase enzyme loading [12,13]. The similar dimensions of the particles and the enzymes enable nanomaterials to operate as an electrical wire decreasing electron transfer distance between the electrode and the active site of the enzymes [14]. Besides, their proximity can possibly accelerate the biocatalytic process. These materials are attractive for sensing and biosensing applications [15], for efficient bioelectrocatalysis [16] and could have a significant role in the development of biofuel cells. Incorporation of carbon nanoparticles (CNPs) is well-established for electrode surface modification in order to improve electron transfer rate between enzymes and electrode surfaces. One simple method involves encapsulation of carbon nanoparticles in organic [17] or inorganic polymer films [18]. Bioelectrodes based on bilirubin oxidase immobilization have been prepared with phenylsulfonated CNPs by layer-by-layer approach [19–21]. The authors showed that the resulting electrode promoted mediatorless bioelectrocatalytic oxygen reduction with good efficiency, as the current densities increased with the amount of deposited nanomaterial. Biocomposite CNP-laccase biocathodes have been prepared by entrapment of CNPs within enzyme polymer matrix for O_2 bioelectrocatalysis [22]. The improved performance was ascribed to the increased amount of enzyme molecules then electronically wired to the electrode through the CNP relays. Carbon Ketjen black was combined with cuperous oxidase [23] or bilirubin oxidase (BOD) [24] for oxygen reduction, or with glucose dehydrogenase (GDH) for glucose oxidation [25], and its developed surface led to increased current densities. Carbon Vulcan was mixed with multicopper oxidases in Nafion to construct efficient bioelectrodes for ethanol biofuel cell [26] and glucose/O_2 biofuel cells [27,28].

To date a few microfluidic BFCs based on immobilized enzymes electrodes and working from glucose as fuel have been developed. One device, composed of a BOD-adsorbed cathode and GDH-adsorbed anode with enzymes encapsulated in polylysine in the presence of Ketjen black, was reported to generate 30 μW cm^{-2} at 0.29 V in an air-saturated solution at pH 7, with a flow rate 1 mL min^{-1} [29]. The originality of this work was the electrode rather smart configuration in a single flow channel. More recently, a microfluidic BFC working from laccase and glucose oxidase covalently bounded onto single-walled carbon nanotube electrodes [30] showed a robust immobilization technique for microfluidic application. The system delivered a maximum power density of 1.65 μW cm^{-2} at 0.235 V. Higher power density generation of 64 μW cm^{-2} at 0.54 V with a flow rate 70 μL min^{-1} was achieved with a microfluidic device using pyrolyzed photoresist film electrodes [31]. The relevance of this work is the combination of thin and flexible films patterned by means of a cutter plotter to build the device, allowing mass production.

Besides, a microfluidic and microfabricated ethanol biofuel cell was developed based on a bioanode composed of a micromolded carbon ink modified with the enzyme alcohol dehydrogenase and methylene green [32]. The bioanode was sealed under a PDMS flow microchannel powering by hydrodynamic flow of ethanol and NAD^+. When the integrated microfluidic bioanode was assembled with an external platinum cathode, the complete biofuel cell produced a maximum power density of 5 μW cm^{-2} at 0.34 V.

This paper describes the development of an ethanol microfluidic BFC based on a biocathode and a bioanode, operating in a Y-shaped microfluidic channel to generate maximum power density. The dimensions and operating conditions of the microfluidic device were such that fluid flow was pressure driven and characterized by very low Reynolds number. At the anode, ethanol was oxidized by alcohol dehydrogenase, whereas at the cathode, the oxygen was reduced by laccase. Electrochemical characterizations of the device were performed by varying the electrode configuration and the flow rate of the streams through the microchannel. In particular, the work focused on the influence of carbon nanoparticles on the electron transfer in attempt to improve efficiency of the bioelectrocatalytic process. The performances of the devices were evaluated from voltage, current density and delivered power density.

2. Experimental

2.1. Materials

Laccase from *Trametes Versicolor* (20 U mg^{-1} solid), Diaphorase (3–20 U mg^{-1}), Alcohol Dehydrogenase (300 U mg^{-1}), β-nicotinamide adenine dinucleotide sodium salt (NAD^+), 2-methyl-1,4-naphthoquinone (VK3), Aceton, polyethylenimine (PEI) (50% (w/v) in H_2O), 2,2′-azinobis(3-ethylbenzothiazoline-6-sulfonate) diammonium salt (ABTS), Nafion® solution (5 wt%), sodium phosphate dibasic dihydrate ($Na_2HPO_4{\cdot}2H_2O$) and sodium phosphate monobasic monohydrate ($NaH_2PO_4{\cdot}H_2O$) were purchased from Sigma–Aldrich and used without further purification. The phosphate buffer was prepared with $Na_2HPO_4{\cdot}2H_2O$ and $NaH_2PO_4{\cdot}H_2O$ (pH 5, 7 or pH 9, 0.1 M). The carbon nanoparticles powder as Super P® and KS6 were purchased from TIMCAL.

2.2. Bioelectrodes preparation

The biocathode to be employed in the electroreduction of oxygen was prepared by adsorption of enzymes and mediators on the surface of the electrodes by drop casting. 333 μL of laccase (15 mg mL^{-1}) and Super P® (15 mg mL^{-1}) in phosphate buffer 0.1 M (pH 5) solution was mixed on a vortex mixer. Sequentially, 100 μL of the solution was mixed with ABTS (5.4 mg mL^{-1}) and 10 μL Nafion®. Then, 6 μL of the preparation was coated onto Au electrode and left to dry at room temperature before keeping in a low humidity environment.

The bioanode to be employed in the oxidation of ethanol was prepared by adsorption of successive coatings separated by a dried step at room temperature. 167 μL of ADH (30 mg mL^{-1}) and KS6 (15 mg mL^{-1}) in phosphate buffer 0.1 M (pH 7) solution was mixed on a vortex mixer and 6 μL of the preparation was pipetted onto the electrode and dried at room temperature. The same procedure was conducted for the immobilization of NAD^+ (30 mg mL^{-1}) and then diaphorase (20 mg mL^{-1}). The last coating on the electrode consisted in pipetting 10 μL of a solution containing VK3 (60 mg mL^{-1}), 190 μL acetone and 10 μL PEI, followed by drying.

2.3. Fabrication of the microfluidic cell

The microfluidic chip was fabricated from a standard soft lithography method described elsewhere [33]. Typically, a glass slide was preliminary cleaned, modified sequentially by three photoresist layers (35 μm Etertec HQ-6100) exposed to UV light through a photomask. The structure was then developed by

spraying an aqueous solution of sodium carbonate (1 wt%) during 4 min and hardened by a second irradiation. The master was then replicated in PDMS at 70 °C during 2 h. After cooling, the PDMS slab was peeled off from the master and holes were punched using a 1.2 mm diameter tube, to provide an access for Teflon tubing. The PDMS slab was then aligned with an epoxy slide containing electrodes. The device consisted of a Y-shaped channel in PDMS with two inlets and two outlets. The microchannel dimensions were: $L = 3$ cm, $w = 2$ mm and $h = 105$ μm (Fig. 1).

The PDMS slab was subsequently sealed to an epoxy substrate that accommodated the electrode pattern. The gold electrodes were deposited by sputtering 300 nm thick Au layer on a 10 nm thick Cr adhesion layer on epoxy substrate. Two electrode patterns with different aspect ratio (length-to-width) were studied (Fig. 2): design (A) with electrodes 5 mm long and 1 mm wide; design (B) with electrodes 10 mm long and 0.5 mm wide. The surface of the gold electrodes in contact with the microfluidic channel was 0.05 cm^2 in both designs.

2.4. Physical characterization

Carbon nanomaterials were analyzed by scanning electron microscopy (SEM, S-4800, Hitachi), and X-Ray diffraction (PANAlyticalXpert-PRO diffractometer equipped with a X'celerator detector using Ni-filtered Cu-radiation). Their electrical conductivity was measured by the four-point probe Van der Pauw method. Their specific surface area was determined, after 2 h outgassing at 200 °C, by applying the BET (Brunauer, Emmett and Teller) equation to the adsorption curve of the N_2 adsorption–desorption isotherms at 77 K (Micromeritics-ASAP 2020).

2.5. Electrochemical measurements

The bioelectrodes were characterized separately by polarization curves performed in 0.1 M phosphate buffer at pH 5 saturated by dioxygen for the biocathode, or in 0.1 M phosphate solution at pH 9 with 160 μL ethanol for the bioanode, after stabilization of the open circuit potential. Electrochemical measurements were performed on a potentiostat Autolab (Eco chemie, Netherlands) at 25 °C in phosphate buffer, with a conventional three-electrodes system composed of a stainless steel auxiliary electrode, a calomel saturated reference electrode and the electrode material as working electrode.

The MBFC was characterized by the same electrochemical equipment. The cathode was connected to the working electrode, and the counter and reference electrodes were both connected to the anode. The catholyte solution consisted of 0.1 M phosphate buffer at pH 5 saturated with O_2. The anolyte solution contained ethanol 160 μL in 0.1 M phosphate buffer at pH 9. Protons diffuse through the liquid–liquid interface created by the contacting streams. The solutions were provided by a syringe pump (Harvad) at variable flow rates and delivered to the cell via tygon tubing.

The open circuit potential (V_{oc}) was measured when no current flowed. An equilibration time was maintained during 5 min before data collection to reach maximum open circuit potential. Polarization curves, known as I–V curves, were obtained by measuring the current while slowly varying the potential between the OCP and 0 V, or by applying external resistances from 100 Ω to 1 MΩ and measuring the resulting current and voltage. Current and power densities were determined using the geometric area of the electrodes.

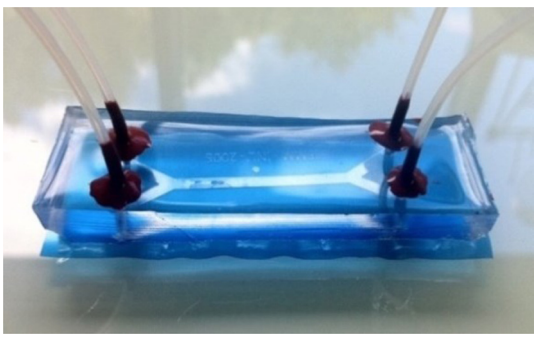

Fig. 1. Photograph of the Y-shaped microfluidic channel in PDMS with two inlets and two outlets.

3. Results and discussion

3.1. Bioelectrodes construction and characterization

The development of the ethanol/O_2 microfluidic BFC requires the construction of bioelectrodes modified by alcohol dehydrogenase and laccase. The catalytic activity of the modified electrodes was first characterized independently prior to the fabrication and characterization of a microfluidic BFC. The immobilization technique was based on the adsorption of enzymes and mediators on the surface of the electrodes by drop casting. The enzymes were previously mixed with carbon black nanomaterials as efficient hosts for enzymes, providing an electrical connection between the enzymes and the electrode, and providing additional surface area for adsorption of active enzymes [12–14]. Two black nanomaterials were tested: carbon Super P® and carbon KS6 characterized by different surface area and electrical conductivity, as indicated in Table 1. SEM and XRD diffraction have been performed on the samples in order to evaluate their structure.

The carbon KS6 is characterized by a sheet structure composed of grain size dimensions of the order of 1 μm (Fig. 3A), and by an intense X-ray diffraction peak at $2\theta = 26°$ typical of graphitic carbon [34] (Fig. 3C). At contrary, the carbon Super P® presents a porous structure composed of smaller nanoparticules of ten nanometers (Fig. 3B) and no characteristic peak on the XRD diffraction pattern. These differences in the structure explain the higher electrical conductivity measured for the carbon KS6 and the specific area 3 times higher for the Super P® that can be built on to construct bioelectrodes. Their impact has been studied on the electrochemical behavior of the bioelectrodes.

Fig. 4A shows the catalytic activity of the bioanode in phosphate buffer solution pH 9 in the presence of ethanol. Ethanol is oxidized to aldehyde by ADH and its cofactor NAD^+. The regeneration of the cofactor is well achieved using an additional redox protein diaphorase which operates efficiently in the presence of the mediator VK3 [35-36]. The electrochemical behavior of the bioanode has been studied in the presence of the different carbon black nanomaterials. The bioanodes exhibit activity for ethanol oxidation with a V_{oc} around −0.43 V/SCE and current densities around 1 mA cm^{-2} (Fig. 4A). A low oxidation current is observed in the absence of the carbon nanomaterials, confirming the formation of effective percolation paths for allowing appropriate electron transport and high amount enzyme loading. However, in the presence of Super P®, a sharp increase of the current density and an oxidation peak at −0.25 V/ECS are observed, corresponding to the oxidation of the mediator VK3.

Fig. 4B shows the electrochemical response of the biocathode towards O_2 electrocatalytic reduction in phosphate buffer at pH 5 and saturated with O_2. From the polarization curves, the oxygen reduction current begins at 0.6 V/ECS, with overpotential of 50 mV, and the current densities feature a semi-plateau that indicates the

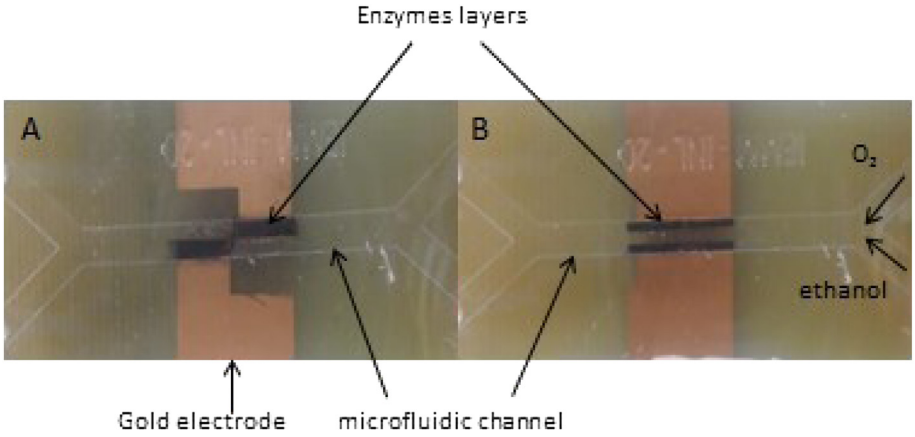

Fig. 2. Photos of gold electrodes ($S = 0.05\ cm^2$) confined within a microfluidic channel (120 high and 2 mm wide) and modified by enzyme layers mixed with carbon nanoparticles, design (A): electrodes 5 mm long × 1 mm wide, and design (B): electrodes 10 mm long × 0.5 mm wide.

Table 1
Physical characteristics of carbon nanomaterials Super P® and KS6 determined by BET and four point contacts method.

Carbon powder	Particle size (μm)[a]	Surface area ($m^2\ g^{-1}$)	Electrical conductivity ($S\ m^{-1}$)
KS6	6	18	30900
Super P	0.04	60	930

[a] Manufacturer data.

control of the electrocatalytic reaction by diffusion of the oxygen to the electrode surface. The biocathode based on Super P® (black curve) shows improved kinetics of the electronic transfer and higher performance increase (500 μA cm^{-2}) in 2-folds compared to biocathode based on KS6.

The first outcome to be observed from polarization curves is that the addition of carbon nanoparticles to the enzyme layers enhances bioelectrocatalytic processes. The large surface area of the nanoparticles enhances the reactive species loading and thus the

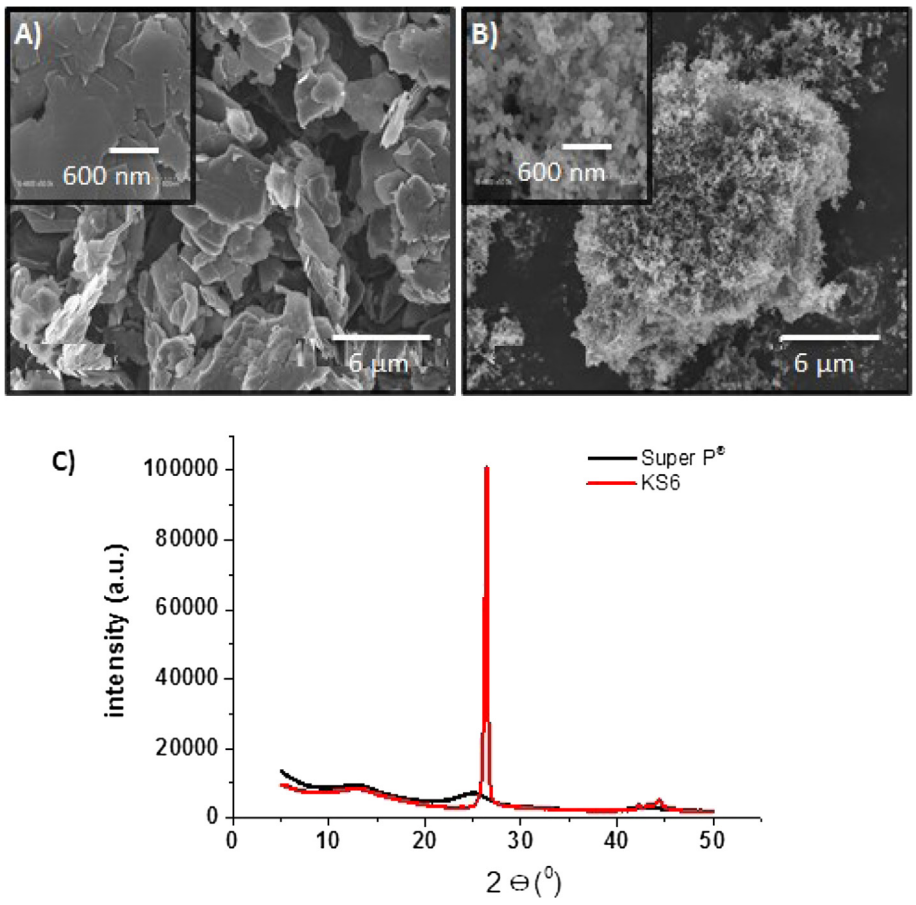

Fig. 3. SEM images of the carbon nanoparticles A) carbon KS6 and B) Super P®; C) XRD pattern of the carbon nanoparticles.

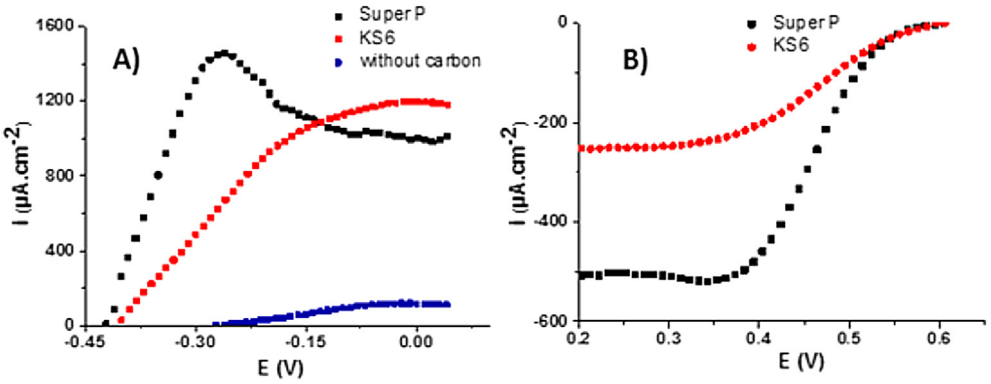

Fig. 4. Polarization curves of (A) bioanodes built without carbon nanomaterials (blue curve), or with carbon KS6 (red curve) or Super P® (black curve), in phosphate solution (pH 9, 0.1 M) with 160 µL ethanol; (B) biocathodes built with the carbon nanomaterials KS6 (red curve), or Super P® (black curve) in O_2-saturated phosphate solution (pH 5, 0.1 M). Scan rate 3.3 mV s^{-1}. (For interpretation of the references to color in this figure legend, the reader is referred to the web version of this article.)

available active sites for electron generation. Besides, the electronic conductivity of the carbon nanoparticles can enhance electron transfer rate to the electrodes. However, it is evident that bioelectrodes based on carbon Super P® display the best performances. The benefit of Super P® may be explained by its high porous structure that offers a close proximity to the reactive species and improves diffusion of ethanol and oxygen within the enzyme films. This assumption was in part corroborated by the structure of the bioelectrodes observed by SEM in the Fig. 5. The bioelectrodes prepared in the absence of nanoparticles present a homogeneous surface without any porosity. However, the presence of the carbon nanoparticles creates a porous film on the electrode surface even more pronounced in the presence of the Super P®.

3.2. Ethanol/O_2 microfluidic BFC

The biocathode was evaluated with respect to the bioanode, and a complete BFC based on a Y-shaped microfluidic channel was tested towards ethanol fuel at room temperature by measuring the optimum power output. To date, only one microchip-based bioanode paired with an external Pt cathode working from ethanol fuel has been developed [32]. This device showed maximal power density of 5 µW cm^{-2} at 0.34 V.

3.2.1. Effect of the Au electrode pattern

A major limitation to obtain high current densities in microfluidic devices is the depletion of fuel and oxidant along the electrode surface, which hinders reaction kinetics and drastically increases the mass transport limitations [37]. Reducing the electrode length can decrease the influence of the boundary layer depletion and thus improve both the current and power densities [38–41]. As the electrodes design confined in the microchannel is an important element in the manufacture of the microfluidic fuel cells, two different electrode patterns with different aspect ratio (see Fig. 2) were tested to assess their influence on the performance of the microfluidic BFC. The total electrode surface and the flow rate were kept constant. Pattern (A) was characterized by electrodes in width that extends over the half of the microchannel, whereas pattern (B) was characterized with narrowed and longer electrodes. It resulted that in pattern (A), the whole solution (anolyte or catholyte) was in contact with the immobilized enzymes while in pattern (B), there was only one part of the solution which showed the immobilized enzymes on electrode surface. Another difference was that in the pattern (A), electrodes are not face-to-face, unlike in pattern (B) and that to avoid contact.

Fig. 6 shows for the different patterns the cell voltage and the resulting power density versus the current density of the ethanol/O_2 microfluidic BFC delivered at the flow rate 16 µL min^{-1}. The device was built from an anode based on carbon nanoparticles KS6 and a cathode based on carbon nanoparticles Super P®. The microfluidic BFC with electrode pattern (A) shows a semi-plateau and a drop in the potential at high current densities typical of mass transfer limitations, whereas the curve shape for the device with electrode pattern (B) shows important ohmic losses and slower kinetics that in turn diminishes V_{oc}. The position of the electrodes influences the ohmic resistance in the microchannel and accounts, at least in part, to the cell performances: electrodes spaced closed to each other (pattern A) allow low internal resistance, whereas the longer gap between bioelectrodes in pattern (B) increases the pathway that protons need to travel from the bioelectrodes [15].

The benefit of the pattern (A) is obvious from the performances of the biofuel cell. The resulting microfluidic BFC delivers the highest V_{oc} (0.8 V) and a power density 80% larger than that found

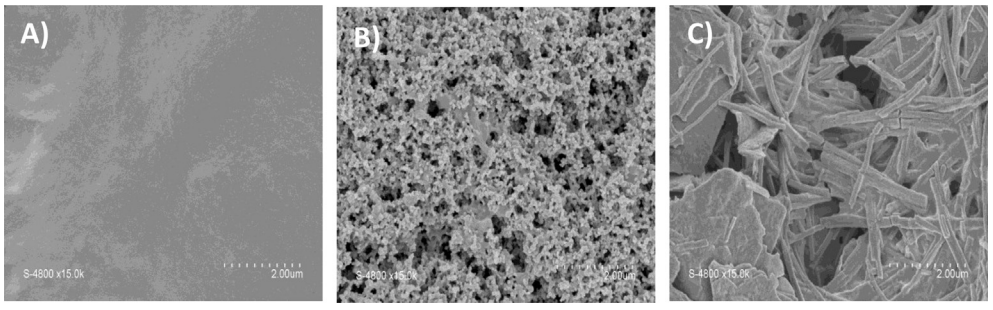

Fig. 5. SEM images of the bioelectrodes prepared in the absence of carbon nanomaterials (A), and in the presence of carbon Super P® (B) and carbon KS6 (C).

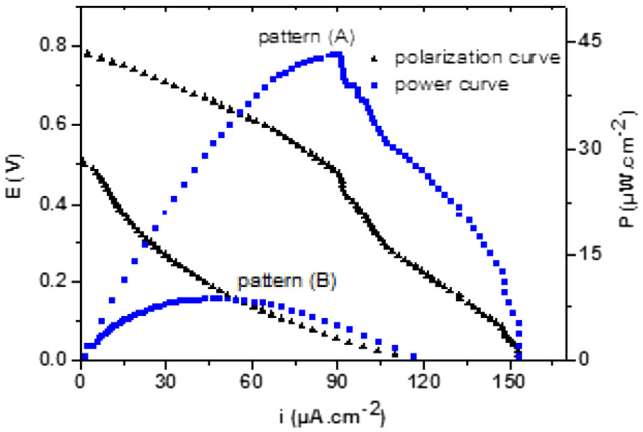

Fig. 6. Polarization (Δ) and power (▫) curves obtained from the ethanol/O_2 MBFC based on KS6 (anode) and Super P® (cathode) with electrode patterns (A) and (B), at flow rate 16 μL min^{-1} with anolyte pH 9/catholyte pH 5 in phosphate buffer 0.1 M, scan rate 3.33 mV s^{-1}.

with the pattern (B) (45 against 10 μW cm^{-2}). Shorter and wider electrodes result in thinner boundary layers and more efficient catalytic consumption of fuel and oxidant at the surface of the electrodes, and thus higher electrode performances. This behavior was also described in the works of Thorson et al. [37] that showed that low aspect ratio (short and wide electrodes) significantly improved the performance of an air-breathing alkaline laminar flow-based fuel cell. We have therefore chosen the microfluidic BFC with pattern (A) for the following work.

3.2.2. Influence of the flow rate

In microfluidic channel, the anolyte and catholyte solutions run in parallel laminar flow, and their interface substitutes for proton exchange membrane separators present in conventional fuel cells [1]. Rapid transport of reactants to the electrodes is essential to provide high power densities. During operation, depletion zones are formed near the electrodes and rapid transport of fuel and oxidant to the electrodes is essential to provide high power densities [3,4,31]. The thickness of the depletion zone increases in the direction of the convective flow and can be regulated by the flow rate of the solutions. Different flow rates were tested: 16, 150 and 300 μL min^{-1} Table 2 shows that the maximum delivered power density did not change significantly with increasing flow rate, indicating that mass transport was not the major limitation. In our case, we rather speculated that the behavior of the power density was mainly due to reaction rate limited in the film, coupled to substrate diffusion at higher current densities. Especially the construction of the bioanode required the deposit of several enzyme/mediator layers that may hamper electron transfer and kinetic oxidation. To further study how to increase the performance of the microfluidic BFC, we selected the lowest flow rate (16 μL min^{-1}) in order to avoid the enzyme layers washed off from the electrodes.

3.2.3. Influence of the carbon nanomaterial structure

It was previously observed that the characteristics of the carbon nanomaterials play a role on the bioelectrode performances. We thus tested a microfluidic BFC built from carbon nanomaterial Super P® mixed with the enzymes at both the bioanode and biocathode, and compare its electrical performance to the previous microfluidic BFC device based on KS6 at the anode and Super P® at the cathode (Fig. 7). The BFC containing the carbon nanomaterial Super P® shows the highest performance increase (90 μW cm^{-2} at 0.6 V) in 2-folds compared to the initial system, supporting a kinetic enhancement of the ethanol oxidation. This result can be attributed to the increased surface area of the anode changing the KS6 by Super P® and therefore to the higher amount of immobilized reactive species on the anode. Besides, the porous structure of the nanoparticles Super P® may promote the proximity of the conductive nanoparticles close to the active site of the active species that possibly reduces the electron transfer distance and accelerates the bioelectrocatalytic process, and thus the power density of the microfluidic BFC. The steady-state behavior of the system was also evaluated from the power curve obtained by applying constant load discharges between 100 Ω and 1MΩ (Fig. 7). In that case, the BFC efficiency is lower due to the equilibrium time to reach the steady state that contributes to the instability of the bioanode [42]. However, the measurement of the current–voltage curves under variable resistances evaluates the potentiality of a microfluidic BFC in real operations.

The evolution of the power density with time and after keeping the electrode in humid atmosphere one night shows quite stable V_{oc} but a pronounced loss of current densities mainly due to the immobilization procedure that was not sufficiently efficient to prevent the leaching of the cofactor NAD^+ and the mediator ABTS (as the adding of the species in solution lead to 85% of the initial electrochemical activity), that contributes to a low stability of the BFC with time. In particular, from additional experiments, the instability resulted mainly from the bioanode. The biocathode lost 20% of its initial current density after 2 weeks, whereas the bioanode lost 80–90% of its initial current density after one day. So it resulted that the microfluidic biofuel cell lost 83% of its initial power density after one day. As described in literature, ethanol-based biofuel cells based on macro-scale electrodes [43–46] or microchip-based bioanode [32] worked with the cofactor NAD^+ in the solution. More works are thus required to get durable and stable microfluidic BFCs. The ethanol/O_2 microfluidic BFC, developed in this work, works from enzymatic reactions performed at

Table 2
Maximal power density as function of flow rate of the MBC (electrode pattern A) built from carbon nanomaterials KS6 at the bioanode and Super P® at the biocathode, with anolyte pH 9/catholyte pH 5 in phosphate buffer 0.1 M.

Flow rate (μL min^{-1})	16	150	300
Maximal power density (μW cm^{-2})	43	44	49

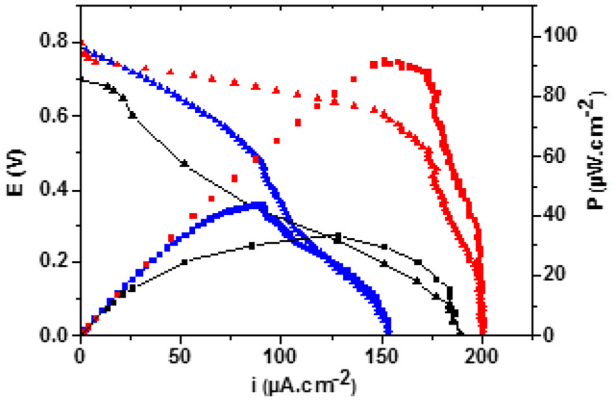

Fig. 7. Polarization (Δ) and power (▫) curves of various MBCs tested with the electrodes pattern A with anolyte pH 9/catholyte pH 5 in phosphate buffer 0.1 M, flow rate = 16 μL min^{-1}. Red curves = MBFC built from bioanode with KS6 and biocathode with Super P®; blue curves = MBFC built from bioanode and biocathode with Super P®; black curves = steady-state behavior of the MBFC (built from Super P®) evaluated on the basis of the cell voltage upon changing the external resistance between 100 Ω and 1 MΩ. (For interpretation of the references to color in this figure legend, the reader is referred to the web version of this article.)

both the cathode and anode with immobilization of the respective enzymes on gold electrodes synthesized by our group. Although comparison with the literature is not straightforward, this ethanol/O_2 BFC delivers a competitive and high power density of 90 μW cm^{-2} with reported microfluidic BFC working from glucose fuel [29–31] or microchip-based bioanode paired with an external Pt cathode working from ethanol fuel [36].

4. Conclusions

This work presented an ethanol microfluidic BFC based on bioelectrodes operating in a Y-shaped microfluidic channel. We showed the enhancement of bioelectrodes electroactivity by carbon nanoparticles as efficient hosts for redox species. The large surface area and the electronic conductivity of the nanoparticles enhance both the reactive species loading and electron transfer rate to the electrodes. Besides, carbon nanoparticles with higher porous structure increased bioelectrocatalytic processes, by offering a closer proximity between the reactive species and the electrode surface, and by improving diffusion of ethanol and oxygen within the enzyme films.

The ethanol microfluidic BFC was optimized as function of the electrode patterns with different aspect ratio. Higher current and power densities were achieved for shorter and wider electrodes that allow for thinner boundary layer depletion at the electrodes surface, resulting in efficient catalytic consumption of fuel and oxidant. The ohmic resistance in the microchannel was reduced by electrodes spaced closed to each other in the microchannel.

This miniaturized device, based on bioelectrodes and working from ethanol, generated the highest maximum power density of 90 μW cm^{-2} at 0.6 V for a flow rate 16 μL min^{-1}. However, the immobilization procedure was not sufficiently efficient to prevent the leaching of the redox mediators NAD^+ and ABTS that contributes to a low stability of the BFC with time. More work is required to get more durable and stable bioelectrodes. In order to produce adequate power for practical applications, we aim to develop a compact fuel cell stack comprising multiple microfluidic biofuel cells.

Acknowledgments

Financial supports by the 'Hybiocell' project in the framework of the ANR program International II and by the European Commission in the framework of an Averroes grant are gratefully acknowledged. Authors would like to thank Jérôme Degouttes and Nicolas Terrier from Nanolyon for Cr/Au electrodes deposition.

References

[1] E. Kjeang, N. Djilali, D. Sinton, Power Sources 186 (2009) 353–369.
[2] J.W. Lee, E. Kjeang, Biomirofluidics 4 (2010) 041301–041312.
[3] J. Yang, S. Ghobadian, P.J. Goodrich, R. Montazami, N. Hashemi, Phys. Chem. Chem. Phys. 15 (2013) 14147–141461.
[4] A. Zebda, L. Renaud, M. Cretin, C. Innocent, F. Pichot, R. Ferrigno, S. Tingry, Power Sources 193 (2009) 602–606.
[5] A. Zebda, L. Renaud, M. Cretin, C. Innocent, R. Ferrigno, S. Tingry, Sensors Actuators B Chem. 149 (2010) 44–50.
[6] F. Davis, S.P. Higson, Biosens. Bioelectron. 22 (2007) 1224–1235.
[7] R.S. Jayashree, S.K. Yoon, F.R. Brushett, P.O. Lopez-Montesinos, D. Natarajan, L.J. Markoski, P.J.A. Kenis, Power Sources 195 (2010) 3569–3578.
[8] D. Fuerth, A. Bazylak, J. Fluids Eng. 135 (2013) 021102–021109.
[9] E.R. Choban, L.J. Markoski, A. Wieckowski, P.J.A. Kenis, Power Sources 128 (2004) 54–60.
[10] R.F. Ismagilov, A.D. Stroock, P.J.A. Kenis, G. Whitesides, H.A. Stone, Appl. Phys. Lett. 76 (2000) 2376–2378.
[11] E.H. Yu, K. Scott, Energies 3 (2010) 23–42.
[12] S.D. Minteer, P. Atanassov, H.R. Luckarift, G.R. Johnson, Mater. Today 15 (2012) 166–173.
[13] S. Ha, Y. Wee, J. Kim, Top. Catal. 55 (2012) 1181–1200.
[14] M. Opallo, R. Bilewicz, Adv. Phys. Chem. (2011) 21.
[15] X. Luo, A. Morrin, A.J. Killard, M.R. Smyth, Electroanalysis 19 (2007) 244–252.
[16] S. Tsujimura, Y. Kamitaka, K. Kano, Fuel Cells 7 (2007) 463–469.
[17] A.M. Zimer, R. Bertholdo, M.T. Grassi, A.J.G. Zarbin, L.H. Mascaro, Electrochem. Commun. 5 (2003) 983–988.
[18] S.M. Macdonald, K. Szot, J. Niedziolka, F. Marken, M. Opallo, Solid State Electrochem. 12 (2008) 287–293.
[19] A. Lesniewski, J. Niedziolka-Jonsson, C. Rizzi, L. Gaillon, J. Rogalski, M. Opallo, Electrochem. Commun. 12 (2010) 83–85.
[20] A. Lesniewski, M. Paszewski, M. Opallo, Electrochem. Commun. 12 (2010) 435–437.
[21] K. Szot, M. Jönsson-Niedziolka, E. Rozniecka, F. Marken, M. Opallo, Electrochim. Acta 89 (2013) 132–138.
[22] U.B. Jensen, M. Vagin, O. Koroleva, D.S. Sutherland, F. Besenbacher, E.E. Ferapontova, Electroanal. Chem. 667 (2012) 11–18.
[23] R. Kontani, S. Tsujimura, K. Kano, Bioelectrochemistry 76 (2009) 10–13.
[24] M. Masuda, Y. Motoyama, K. Murata, N. Nakamura, H. Ohno, Electroanalysis 23 (2011) 2297–2301.
[25] M. Ammam, J. Fransaer, Biotechnol. Bioeng. 109 (2012) 1601–1609.
[26] L.N. Akers, M.C. Moore, D.S. Minteer, Electrochim. Acta 50 (2005) 2521–2525.
[27] A. Habrioux, K. Servat, S. Tingry, K.B. Kokoh, Electrochem. Commun. 11 (2009) 111–113.
[28] G. Gupta, C. Lau, B. Branch, V. Rajendran, D. Ivnitski, P. Atanassov, Electrochim. Acta 56 (2011) 10767–10771.
[29] M. Togo, A. Takamura, T. Asai, H. Kaji, M. Nishizawa, Power Sources 178 (2008) 53–58.
[30] T. Beneyton, I.P.M. Wijaya, C. Ben Salem, A.D. Griffiths, V. Taly, Chem. Commun. 49 (2013) 1094–1098.
[31] M.J. González-Guerrero, J.P. Esquivel, D. Sánchez-Molas, P. Godignon, F.X. Muñoz, F. Javier del Campo, F. Giroud, S.D. Minteer, N. Sabaté, Lab. Chip 13 (2013) 2972–2979.
[32] C.M. Moore, S.D. Minteer, R.S. Martin, Lab. Chip 5 (2005) 218–225.
[33] A. Zebda, J. Renaud, M. Cretin, F. Pichot, C. Innocent, R. Ferrigno, S. Tingry, Electrochem. Commun. 11 (2009) 592–595.
[34] T. Szabo, A. Szeri, I. Dékany, Carbon 43 (2005) 87–94.
[35] H. Sakai, T. Nakagawa, Y. Tokita, T. Hatazawa, T. Ikeda, S. Tsujimura, K. Kano, Energy Environ. Sci. 2 (2009) 133–138.
[36] G. Li, J. Hao, Electrochem. Soc. 156 (2009) 134–138.
[37] M.R. Thorson, F.R. Brushett, C.J. Timberg, P.J.A. Kenis, Power Sources 218 (2012) 28–33.
[38] S.K. Yoon, G.W. Fichtl, P.J.A. Kenis, Lab. Chip 6 (2006) 1516–1524.
[39] A. Bazylak, D. Sinton, N. Djilali, Power Sources 143 (2005) 57–66.
[40] A.E. Khabbazi, A.J. Richards, M. Hoorfar, Power Sources 195 (2010) 8141–8151.
[41] S. Topcagic, S.D. Minteer, Electrochim. Acta 51 (2006) 2168–2172.
[42] D. Selloum, A. Abou Chaaya, M. Bechelany, V. Rouessac, P. Miele, S. Tingry, Mater. Chem. A 2 (2014) 2794–2800.
[43] L. Deng, L. Shang, D. Wen, J. Zhai, S. Dong, Biosens. Bioelectron. 26 (2010) 70–73.
[44] S.A. Neto, J.C. Forti, V. Zucolotto, P. Ciancaglini, A.R. de Andrade, Biosens. Bioelectron. 26 (2011) 2922–2926.
[45] D.E. Gutiérrez-Domínguez, D.E. Pacheco-Catalán, R. Patiño-Diaz, B. Canto-Canché, M.A. Smit, Hydrogen Energy 38 (2013) 12610–12616.
[46] S.A. Neto, T.S. Almeida, L.M. Palma, S.D. Minteer, A.R. de Andrade, Power Sources 259 (2014) 25–32.